

Transmission- and side-detection configurations in ultrasound-modulated optical tomography of thick biological tissues

Jun Li, Sava Sakadžić, Geng Ku, and Lihong V. Wang

Ultrasound-modulated optical tomography of thick biological tissues was studied based on speckle-contrast detection. Speckle decorrelation was investigated with biological tissue samples of various thicknesses. Images of optically absorbing objects buried in biological tissue samples with thicknesses up to 50 mm were obtained in a transmission-detection configuration. The image contrast was more than 30%, and the spatial resolution was approximately 2 mm. In addition, a side-detection scheme along with two specific configurations were examined, and the advantages were demonstrated. Experimental results implied feasibility of applying the ultrasound-modulation technique to characterize optical properties in inhomogeneous biological tissues. © 2003 Optical Society of America

OCIS codes: 170.3880, 120.6150, 110.7050, 110.7170.

1. Introduction

Ultrasound-modulated optical tomography, which is a hybrid technique that takes advantage of both optical contrast and ultrasonic resolution, is an attractive emerging technique in the biomedical optical imaging field. Because biological tissues are optically turbid media, light is strongly scattered inside them. In purely optical imaging, sophisticated reconstruction algorithms are usually required to achieve good imaging depth and reasonable resolution. In ultrasound-modulated optical tomography, an ultrasonic wave is focused into the tissue to modulate the light passing through the ultrasonic focal zone. The modulated or tagged light carries the ultrasonic frequency and, therefore, can be discriminated from the background unmodulated light. Because ultrasonic waves are scattered less in biological tissues than are light waves, the origins of the tagged light can be directly derived from the position of the ultrasonic column inside the tissue. By scanning the ultrasonic beam or the tissue sample, an

image related to local optical properties inside the tissue can be reconstructed.

Ultrasound-modulated optical tomography has been studied for several years. Wang *et al.*¹ and Wang and Zhao² studied ultrasound-modulated optical tomography with continuous-wave ultrasound and obtained images in tissue-simulating turbid media. Wang and Ku³ employed a frequency-swept technique to achieve controllable spatial resolution along the ultrasonic axis. Leveque *et al.*⁴ and Leveque-Fort⁵ developed a parallel speckle detection scheme and obtained three-dimensional images of biological tissues. With this technique, Yao and Wang⁶ and Yao *et al.*⁷ obtained two-dimensional (2D) images of multiple objects buried in biological tissues and further developed the technique by combining parallel detection with frequency-swept techniques. Recently, Li and Wang⁸ modified the parallel detection mode by reducing the acquisition time and improving the signal-to-noise ratio (SNR). In addition to the work conducted on transmission configurations, imaging in reflection configurations has also been studied.^{9–12} More recently, Selb, *et al.*¹³ explored nonlinear effects in imaging. Li *et al.*¹⁴ applied speckle-contrast detection in tomography and obtained 2D images of biological-tissue samples up to 25 mm thick. Ultrasonic modulation mechanisms have been well explained by Wang^{15,16} and Sakadžić and Wang¹⁷ with comprehensive analytic and Monte Carlo models.

To meet the requirements of practical applications,

The authors are with the Optical Imaging Laboratory, Department of Biomedical Engineering, Texas A&M University, 3120 TAMU, College Station, Texas 77843-3120. L. V. Wang's e-mail address is lwang@tamu.edu.

Received 31 October 2002; revised manuscript received 11 March 2003.

0003-6935/03/194088-07\$15.00/0

© 2003 Optical Society of America

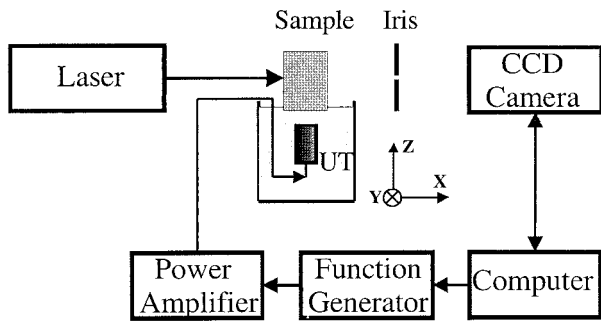


Fig. 1. Schematic of experimental setup. UT, ultrasonic transducer.

researchers will undoubtedly continue for a long time the quest to improve image quality and to increase imaging depth. In this paper, we report our recent experimental study on thick-biological-tissue tomography. Speckle decorrelation was studied, and time-dependent correlation coefficients of speckle patterns were measured at various sample thicknesses. The corresponding speckle contrasts of the speckle patterns were checked. Through the use of speckle-contrast detection,¹⁴ to which we added some improvements, we implemented imaging experiments with tissue samples of thicknesses ranging from 40 to 50 mm in a transmission-detection configuration. In addition, we proposed side-detection configurations. Images obtained with side-detection configurations were compared with those obtained with transmission-detection configuration as well as with those obtained with reflection-detection configuration (reported by other researchers¹²). For the side-detection configuration technique, initial experiments were carried out to check the sensitivity of ultrasound-modulated optical tomography for discriminating objects of different optical absorption properties and for measuring distributions of the ultrasound-modulated signal inside a tissue sample to characterize the tissue's optical properties.

2. Experimental Setup

The setup, which is similar to that described in previous research,¹⁴ is shown in Fig. 1. In the current experiments, a tunable Ti:Sapphire laser (Coherent Inc. 890) operating at 786 nm was applied; we took advantage of its power (~ 140 mW) and its coherence length (over 30 m). The laser beam was expanded to ~ 14 mm in diameter before it was incident on the samples. The resulting power density was ~ 91 mW/cm², which is within the safety limit.¹⁸ Continuous ultrasonic waves were generated with a focused transducer (Ultran VHP100-1-R38), which had a 38-mm focal length and a 1-MHz central response frequency. Dimensions of the focal zone were ~ 20 mm along the ultrasonic axis and ~ 2 mm laterally. The peak pressures in the focal zone were $\sim 10^5$ Pa. A 12-bit CCD camera of 256×256 pixels (Dalsa CA-D1-0256T) was used to detect speckle patterns generated by scattered light transmitted through the

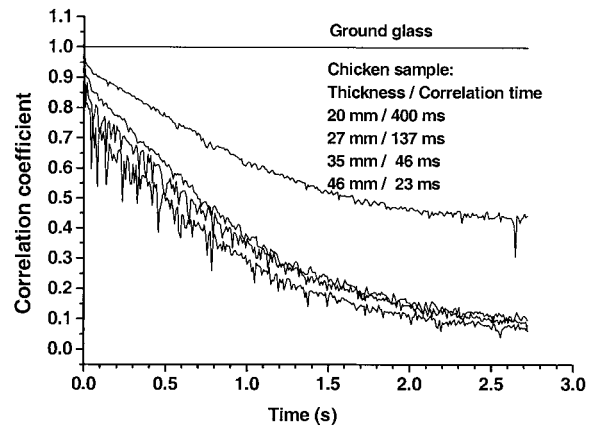


Fig. 2. Time-dependent correlation coefficients of speckle patterns generated with chicken breast tissues of various thicknesses. The result of ground-glass sample is shown for comparison.

sample. An iris was placed before the CCD camera to control the average speckle size on the CCD surface. In association with the adjustment of the iris aperture, the CCD exposure time was set to ensure that sufficient photons would be collected without decorrelation of speckle patterns. A computer was applied to control the CCD camera for implementing optical detection and for data transference. The computer also controlled a function generator that generated electrical signals, which were amplified by a power amplifier and then sent to drive the transducer. Speckle contrasts were measured under conditions with and without ultrasound modulation, and the differences in the speckle contrasts were taken as imaging signals, which were related to the ultrasound modulation depth.¹⁴

3. Experimental Results and Discussion

Because biological tissues were used in our experiments, speckle noise, which is an intrinsic factor in tissue experiments, became a significant noise source in the signal detection. Movements of small particles inside biological tissue, e.g., Brownian motion, cause the noise, which leads to decorrelation of laser speckle patterns. To check the speckle pattern decorrelation, we measured correlation coefficients between speckle patterns within a time period of ~ 2.8 s. Three hundred frames of speckle patterns were sequentially acquired with the CCD camera within the time period. The CCD exposure time was ~ 9 ms. Chicken-breast-tissue samples of various thicknesses were used (Fig. 2). Because speckle pattern decorrelation is sensitive to movements of any of the components in the experimental setup, we did a measurement with a ground-glass sample first to check the setup. The result is presented in the figure. The correlation coefficient measured with the ground-glass sample did not change with time, maintaining a value of ~ 1 , which indicated that the setup was stable enough for our purposes. The results from the chicken samples show that the correlation coefficients decrease rapidly as time elapses. Spe-

cifically, with the increase of sample thickness, the correlation coefficient decrease becomes more significant. Some spikelike fluctuations are seen in the curves, which are more remarkable in the thicker-tissue experiments. By checking the experimental system and comparing the results with those from the ground-glass sample, we conclude that the fluctuations were caused by mechanical disturbances affecting the sample. The disturbance led to recoverable movements of photon scatters inside the tissue, which led to recoverable changes of the speckle patterns. Because it is soft, chicken tissue is more subject to mechanical disturbances, e.g., shape distortion, than the ground glass. Therefore, the fluctuation of the correlation coefficient was significant in the tissue samples. Since the photons had longer path lengths in thicker tissues, the influence of the disturbance was more significant and, as a consequence, the fluctuation was more remarkable in the thicker tissue samples. We define correlation time as the time period after which the correlation coefficient decreases from 1 to 0.8. The correlation time for the samples of thicknesses 20, 27, 35, and 46 mm were found to be 400, 137, 46, and 23 ms, respectively. The data imply that tomography of thick-biological-tissue samples based on a CCD camera of a limited maximum frame rate is challenging. The maximum frame rate of our CCD camera is ~ 200 frames/s. Because sufficient exposure is required, in practice the frame rate is usually lower. We had thought that speckle decorrelation would be much more significant in thick-biological-tissue experiments, and the data do, in fact, verify our suppositions. In parallel speckle detection, a four-frame acquisition⁴⁻⁸ or a two-frame acquisition⁸ is needed and the acquired frames must be correlated. For experiments in which the detection is used, the sample thickness are limited because of speckle decorrelation. We also expected that speckle-contrast detection would be efficient in thick-sample experiments, and we checked it experimentally (as we report here).

The speckle contrasts of the speckle patterns, which were studied in Fig. 2, were measured as functions of time. Measurements of samples with various thicknesses have similar results; there is no tendency indicating that speckle contrast varies with time, although the speckle contrast does fluctuate in measurements taken at different moments. Figure 3 shows the results with a 20-mm sample. With the increase of the sample thickness, the fluctuation becomes slightly significant. However, the fluctuation, which we define as the ratio of the standard deviation to the mean, increases slowly with sample thickness. It is only $\sim 1\%$ in the case of a 46-mm sample. The speckle contrasts measured under ultrasound modulation for the 20-mm sample are also shown in the figure. Compared with the results without ultrasound modulation, the only difference is that the speckle contrasts are lower under ultrasound modulation. It has been recognized¹⁴ that the variation in speckle contrast with ultrasound modu-

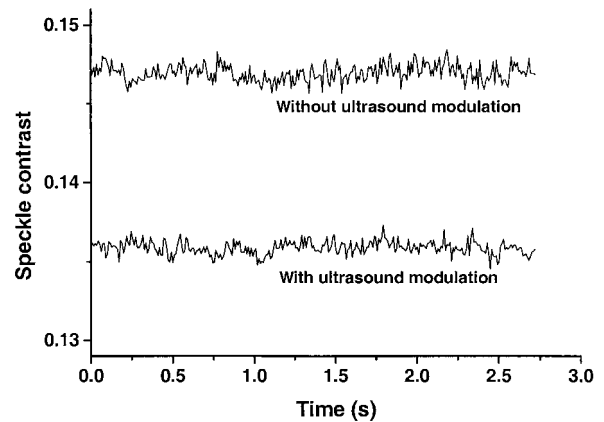
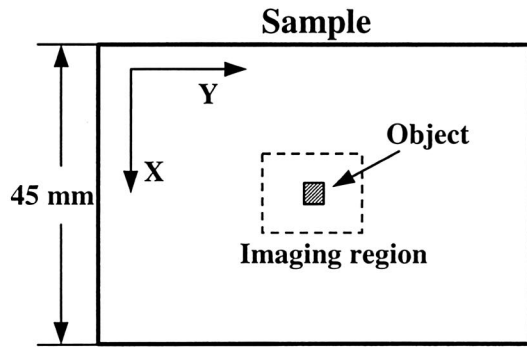


Fig. 3. Speckle contrasts versus time. The results of a 20-mm-thick chicken sample, which were obtained without and with ultrasound modulation are compared.

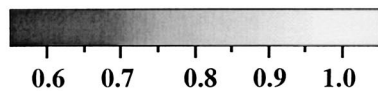
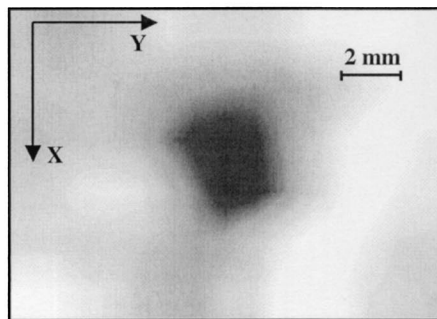
lation is related to the ultrasound-modulation depth, and it can, therefore, be used as an imaging signal. In the case of thick-sample imaging, the speckle-contrast measurement shows distinctive advantages; it needs only a one-frame acquisition to obtain speckle contrast, and an average can be done over multiple independent acquisitions to obtain a mean value. Although the fluctuation of speckle contrast becomes somewhat significant for thick samples, sufficient SNRs for imaging can still be obtained by averaging the speckle contrasts, provided the ultrasound modulation depth is high enough.

By employing speckle-contrast detection, imaging experiments with thick-biological-tissue samples were carried out in a transmission-detection configuration. The tissue samples were made of chicken breast tissue, and the objects buried in the tissue were soft rubber, which had good acoustic coupling with the tissue and little acoustic absorption. The objects were buried in the middle plane of the sample. To obtain a 2D image, we scanned the transducer and the sample along the X and the Y directions, respectively. At each scanning position, 200 measurements were made respectively with, and without, ultrasound modulation. The results were averaged. In this study, speckle-contrast detection¹⁴ was improved, and efforts were made to monitor the SNRs and ensure that the detected signals had SNRs over unity. The mean and the standard deviation of the speckle contrasts obtained from each of the 200 measurements were checked for both cases—with and without ultrasound modulation. If the difference of the means (i.e., the imaging signal) was less than the sum of two standard deviations, which we defined as noise, the imaging signal was discarded, and another 200 measurements were repeated until the signal was larger than the sum of the standard deviations, i.e., $\text{SNR} > 1$.

While applying the above rule for accepting or rejecting the imaging signal, we obtained images of thick samples with single, as well as double objects. Figure 4(a) shows a sketch of a 45-mm-thick chicken



(a)

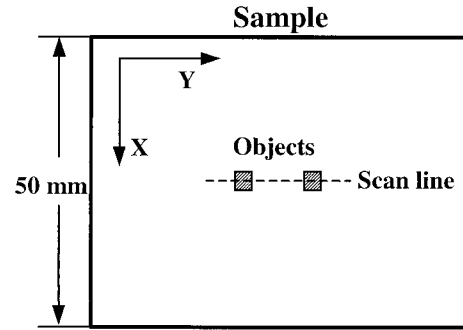


(b)

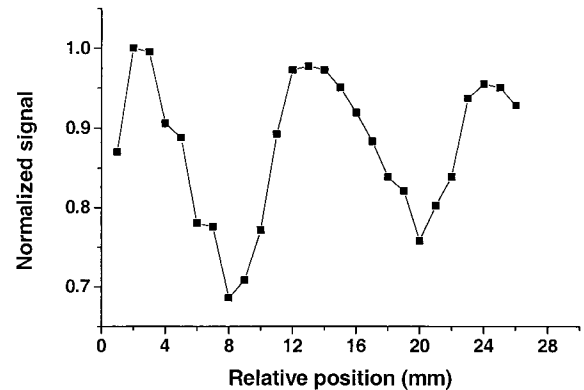
Fig. 4. (a) Sketch of a 45-mm-thick chicken-breast-tissue sample. An object is buried in the middle of the sample. The relative sizes of the object, imaging region and the whole sample are shown. (b) A 2D image of the object. The image was obtained with the transmission-detection configuration.

sample, in which a buried object ($3.5 \text{ mm} \times 3.1 \text{ mm} \times 14.9 \text{ mm}$, along the X , Y , and Z directions, respectively), imaging region, and the whole sample are drawn proportionally. Figure 4(b) shows a clear 2D image of the object. The SNRs in the measurement are ~ 3 . Figure 5(a) shows a sketch of a 50-mm-thick chicken sample, in which two buried objects ($3.5 \text{ mm} \times 3.1 \text{ mm} \times 15.2 \text{ mm}$ and $3.3 \text{ mm} \times 3.1 \text{ mm} \times 15.2 \text{ mm}$, respectively) and the whole sample are drawn to scale and a scan line along the Y axis at the center of the sample is shown. Figure 5(b) shows a one-dimensional (1D) image corresponding to the scan line indicated in Fig. 5(a). Two dips showing the objects are sharp in the figure. It should be noted that with such a thick sample, the image contrast is still quite good, up to $\sim 30\%$. Also, the spatial resolution is approximately 2 mm, close to the size of the ultrasonic focal spot.

In addition, we proposed a detection mode that we



(a)



(b)

Fig. 5. (a) Sketch of a 50-mm-thick chicken-breast-tissue sample. Two objects are buried in the middle of the sample. (b) A 1D image corresponding to the scan line indicated in (a), which is along the Y axis at the center of the sample. The image was obtained with the transmission-detection configuration.

called side detection, which is an intermediate modality between the transmission and the reflection mode. Figures 6(a) and 6(b) show two configurations, respectively, in which the CCD camera and the transducer were placed at two opposite sides of the

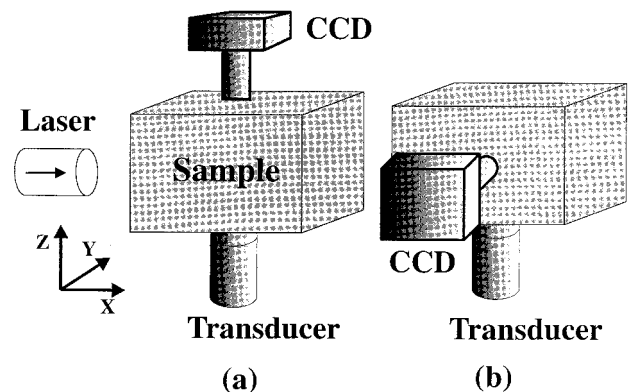


Fig. 6. Schematic of side-detection configurations. (a) The CCD camera and the transducer are located at two opposite sides of the sample. (b) The CCD camera is located at an angle of 90° to the transducer.

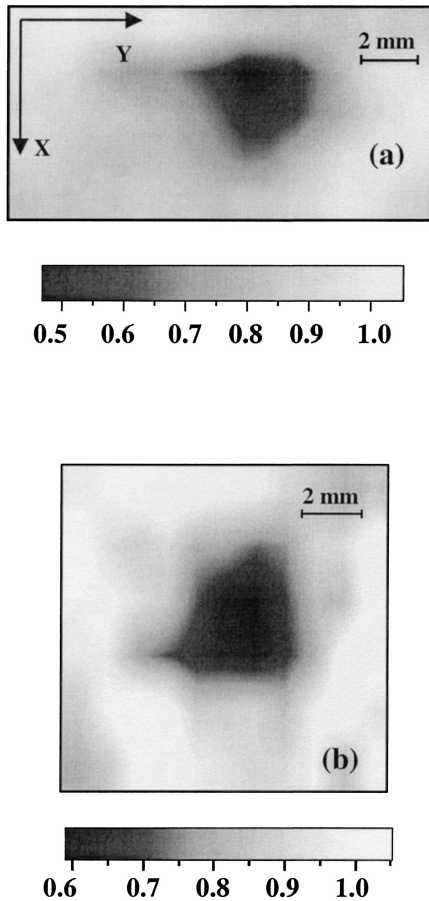


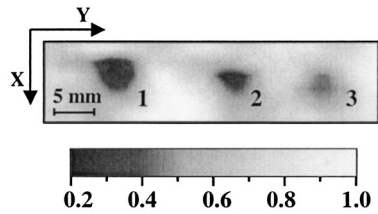
Fig. 7. Two-dimensional images obtained with side-detection configurations. (a) The image was obtained with the configuration shown in Fig. 6(a). The object was buried in the middle of a chicken-breast-tissue sample (size of 40 mm \times 65 mm \times 50 mm). (b) The image was obtained with the configuration shown in Fig. 6(b). The object was buried 12 mm deep in the X direction in a chicken-breast-tissue sample (size of 43 mm \times 65 mm \times 50 mm).

sample or the CCD was at an angle of 90° to the transducer. The configuration in Fig. 6(a) was examined with an imaging experiment with a thick chicken sample (40 mm \times 65 mm \times 50 mm along the X , Y , and Z directions, respectively). An object of 3 mm \times 3 mm \times 13.8 mm was buried in the middle of the sample. To obtain a 2D image required that the transducer be scanned along the X axis and that the sample be scanned along the Y axis, respectively. Figure 7(a) shows a 2D image of the buried object. The size of the object in the image agrees with the real size, and the image contrast is high (up to $\sim 50\%$). In the configuration shown in Fig. 6(b), the incident laser, the CCD camera, and the transducer were at an angle of 90° to each other. The arrangement is more compact and convenient for application. The configuration was examined with an experiment that employed a chicken sample of 43 mm \times 65 mm \times 50 mm. An object of 3.1 mm \times 3.0 mm \times 14.1 mm was buried 12 mm deep in the sample in the X direction. The transducer and the sample were scanned along the X axis and the Y axis, respectively. A clear

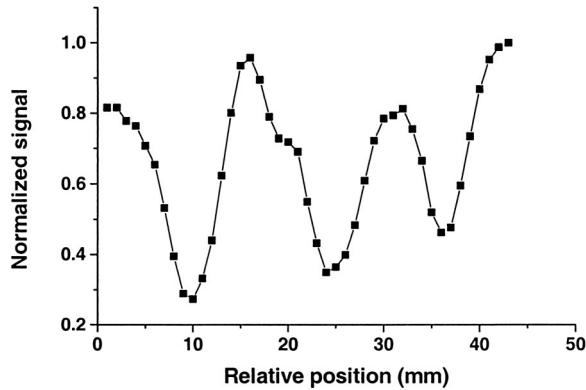
image of the object was obtained, which is shown in Fig. 7(b). These results indicate that detection is nearly identical at any position around the sample because light is diffused after experiencing sufficient scattering in the thick-tissue samples. In the experiment of Leveque *et al.*¹² in which they used a reflection configuration, they obtained an image with a significant shadow, which was inferior to the image obtained with the transmission configuration. Our results show that the images obtained in the side-detection configurations have similar qualities to those obtained in the transmission configuration. For application, side detection is a more convenient configuration than transmission detection. Since the reflection configuration reported on so far placed the transducer at the side of sample, the side-detection configuration actually has the same convenience as reflection configuration. In addition, the strong surface reflection of light, which is significant in the reflection mode, is avoided in side detection. This should lead to a higher SNR in side detection. In other words, side-detection configuration can be applied as an alternative to the reflection configuration.

With the side-detection configuration shown in Fig. 6(a), we tested the sensitivity of ultrasound-modulated optical tomography for identifying objects with different optical absorption properties. A chicken sample (43 mm \times 65 mm \times 50 mm, along the X , Y , and Z directions, respectively) with three objects, which were buried in a plane 15 mm deep in the X direction, was used. The objects were soft white rubber, with identical sizes (3 mm \times 3 mm \times 14 mm). Surfaces of two of the objects were stained with black and green dyes, respectively, which led to differences in optical absorption between the objects; the black one had the strongest absorption, and the one that was left (white) had the weakest absorption. A 2D image of the objects is shown in Fig. 8(a) and a 1D image corresponding to a scan line across the objects along the Y axis is shown in Fig. 8(b). The black, the green, and the white objects are seen with different contrasts, which reflect the optical absorption correctly: the stronger the absorption, the higher the contrast. In detail, the contrast of the black one is $\sim 12\%$ and $\sim 35\%$ higher than that of the green one and the white one, respectively. It is seen that the differences in optical absorption from the objects' surfaces led to significant differences in image contrasts. This initial test shows that ultrasound-modulated optical tomography has good sensitivity for discriminating objects with different absorption properties.

Further, with the side-detection configuration, we measured the modulated signal, i.e., speckle-contrast difference along the X direction inside the tissue, which reflected photon density distribution. The measurement attempted to use the configuration to characterize the optical properties (absorption and scattering) of the biological-tissue samples. In this experiment, we used a diode laser (Melles Griot 561MS667; wavelength, 690 nm; coherence length, over 1 m). For the measurements, the CCD camera



(a)



(b)

Fig. 8. (a) Two dimensional image of three objects of different optical absorption: 1, black-surface object; 2, green-surface object; 3, (original) white-surface object. The image was obtained with the configuration shown in Fig. 6(a). (b) A 1D image corresponding to a scan line across the objects along the Y axis.

and the transducer were kept fixed, and a thick chicken sample in a cubic shape ($47 \text{ mm} \times 65 \text{ mm} \times 50 \text{ mm}$) was scanned along the X direction. According to diffusion theory, the photon fluence rate $\psi(x)$ deep inside a turbid medium decays exponentially with the distance x from the source, i.e., $\psi(x) \propto \exp(-\mu_{\text{eff}} x)$, where $\mu_{\text{eff}} = (3\mu_a\mu_s')^{1/2}$ is the effective attenuation coefficient, and μ_a and μ_s' are the absorption coefficient and the reduced scattering coefficient, respectively. By measuring the photon density distribution and fitting it with the above exponential function, one can obtain the effective attenuation coefficient.

Figure 9 shows a measured signal distribution—a decay curve. But it is not smooth as expected; instead, the curve is composed of several segments. In each segment, the curve decays with the distance x . And at each interface between two segments, fluctuations occur. We repeated the measurement several times and obtained similar results that seemed to reflect a real distribution of the transmitted photons inside the sample. For comparison, we measured the signal distribution with a gel sample, which was uniform in structure and optical properties. The result showed a smooth decay curve without fluctuations. The chicken sample used in the experiment was made of chicken breast slices with different

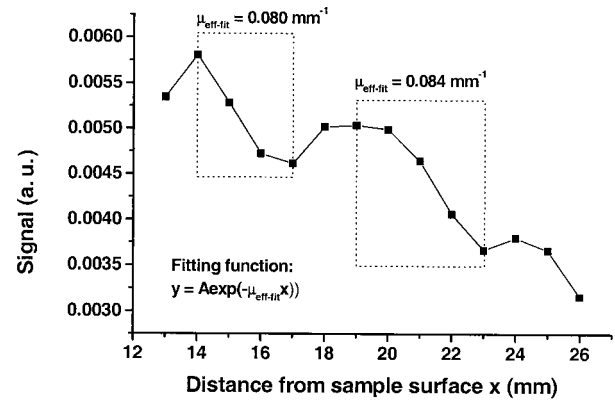


Fig. 9. Measured modulated signal distribution along the X direction inside a chicken-breast-tissue sample. Fitting the data in each segment in the distribution with the 1D model of diffusion theory permitted effective attenuation coefficients of the sample to be deducted.

thicknesses. The measured signal fluctuations were found to be located at each interface between two slices. We prepared the sample carefully and tried to avoid presence of air bubbles between the slices, which could cause changes in acoustic impedance at the interfaces and induce signal fluctuations. We believe that the signal fluctuations reflected the photon distribution at the interfaces and the layer structure of the sample. We tried to fit the data of each segment in Fig. 9 with an exponential decay function and obtained effective attenuation coefficients of 0.80 cm^{-1} and 0.84 cm^{-1} for the two segments; these measurements agree with those reported by Marquez *et al.*¹⁹ According to the measurements of Marquez *et al.*, μ_a and μ_s' of chicken breast tissue at wavelength of 690 nm are $\sim 0.1 \text{ cm}^{-1}$ and $\sim 2.2 \text{ cm}^{-1}$, respectively. The corresponding effective attenuation coefficient is 0.81 cm^{-1} . The results show that the optical properties (i.e., μ_{eff}) of different layers in the tissue sample could be determined individually by measurement of ultrasound-modulated signals. Lev and Sfez¹⁰ claimed successful application of this measurement in determining the optical properties of homogeneous turbid medium. Our experiment with a layer-structure tissue sample, together with the above sensitivity experiment, indicates that the ultrasound-modulation technique offers promise for the determination of spatially resolved optical properties in complicated inhomogeneous biological-tissue samples.

4. Conclusion

The ultrasound-modulated optical tomography of thick biological tissues was studied. Speckle decorrelation was investigated with samples of various thicknesses, and the speckle-contrast detection in thick-biological-tissue tomography was shown to have advantages over other techniques. With the resulting improved speckle-contrast measurement, images of biological tissue samples of thicknesses up to 50 mm were successfully obtained in a

transmission-detection configuration. This thickness is the maximum so far reported for ultrasound-modulated optical tomography. The image contrast was up to 30%, and the image resolution was ~ 2 mm, which was determined by the ultrasonic focal spot size.

Side-detection configurations were proposed, which are more convenient than transmission configuration for practical applications and can be applied as alternatives to the reflection configuration. Experimental results showed that the images obtained with side-detection configurations had similar qualities to those obtained with transmission configuration, and they were far superior to images obtained with reflection-detection configuration. Further, two experiments were conducted with side-detection configuration to test the sensitivity of the ultrasound-modulated optical tomography for discriminating objects of different optical absorption and for measuring optical properties in a layer-structure sample, respectively. The results from these two experiments implied that the ultrasound-modulation technique is a promising one for characterizing the optical properties of complicated inhomogeneous tissue samples.

This project was sponsored in part by National Science Foundation grant BES-9734491, Texas Higher Education Coordinating Board grant 000512-0063-2001, and National Institutes of Health grant R01 EB000712.

References

1. L.-H. Wang, S. L. Jacques, and X. Zhao, "Continuous-wave ultrasonic modulation of scattered laser light to image objects in turbid media," *Opt. Lett.* **20**, 629–631 (1995).
2. L.-H. Wang and X. Zhao, "Ultrasound-modulated optical tomography of absorbing objects buried in dense tissue-simulating turbid media," *Appl. Opt.* **36**, 7277–7282 (1997).
3. L.-H. Wang and G. Ku, "Frequency-swept ultrasound-modulated optical tomography of scattering media," *Opt. Lett.* **23**, 975–977 (1998).
4. S. Leveque, A. C. Boccara, M. Lebec, and H. Saint-Jalmes, "Ultrasonic tagging of photon paths in scattering media: parallel speckle modulation processing," *Opt. Lett.* **24**, 181–183 (1999).
5. S. Leveque-Fort, "Three-dimensional acousto-optic imaging in biological tissues with parallel signal processing," *Appl. Opt.* **40**, 1029–1036 (2000).
6. G. Yao and L.-H. Wang, "Theoretical and experimental studies of ultrasound-modulated optical tomography in biological tissue," *Appl. Opt.* **39**, 659–664 (2000).
7. G. Yao, S. Jiao, and L.-H. Wang, "Frequency-swept ultrasound-modulated optical tomography in biological tissue by use of parallel detection," *Opt. Lett.* **25**, 734–736 (2000).
8. J. Li and L.-H. V. Wang, "Methods for parallel-detection-based ultrasound-modulated optical tomography," *Appl. Opt.* **41**, 2079–2084 (2002).
9. A. Lev, Z. Kotler, and B. G. Sfez, "Ultrasound tagged light imaging in turbid media in a reflectance geometry," *Opt. Lett.* **25**, 378–380 (2000).
10. A. Lev and B. G. Sfez, "Direct, noninvasive detection of photon density in turbid media," *Opt. Lett.* **27**, 473–475 (2002).
11. E. Granot, A. Lev, Z. Kotler, and B. G. Sfez, "Detection of inhomogeneities with ultrasound tagging of light," *J. Opt. Soc. Am. A* **18**, 1962–1967 (2001).
12. S. Leveque-Fort, J. Selb, L. Pottier, and A. C. Boccara, "In situ local tissue characterization and imaging by backscattering acousto-optic imaging," *Opt. Commun.* **196**, 127–131 (2001).
13. J. Selb, L. Pottier, and A. C. Boccara, "Nonlinear effects in acousto-optic imaging," *Opt. Lett.* **27**, 918–920 (2002).
14. J. Li, Geng Ku, and L.-H. V. Wang, "Ultrasound-modulated optical tomography of biological tissue using contrast of laser speckles," *Appl. Opt.* **41**, 6030–6035 (2002).
15. L.-H. V. Wang, "Mechanisms of ultrasonic modulation of multiply scattered coherent light: an analytic model," *Phys. Rev. Lett.* **87** (043093) 1–4 (2001).
16. L.-H. V. Wang, "Mechanisms of ultrasonic modulation of multiply scattered coherent light: a Monte Carlo model," *Opt. Lett.* **26**, 1191–1193 (2001).
17. S. Sakadžić and L.-H. V. Wang, "Ultrasonic modulation of multiply scattered coherent light: an analytical model for anisotropically scattering media," *Phys. Rev. E* **66** (026603) 1–9 (2002).
18. American National Standards Institute, *American National Standard for the Safe Use of Lasers in Health Care Facilities. Standard Z136.1-2000*. (ANSI, Inc., New York, 2000).
19. G. Marquez, L.-H. V. Wang, S. P. Lin, J. A. Schwartz, and S. L. Thomsen, "Anisotropy in the absorption and scattering spectra of chicken breast tissue," *Appl. Opt.* **37**, 798–804 (1998).